Ocean-Induced Melt Triggers Glacier Retreat in Northwest Greenland

M. Wood, E. Rignot, I. Fenty, D. Menemenlis, R. Millan, M. Morlighem, J. Mouginot, H. Seroussi

Ocean-Induced Melt Triggers Glacier Retreat in Northwest Greenland

M. Wood[1] , **E. Rignot**[1] , **I. Fenty**[2] , **D. Menemenlis**[2] , **R. Millan**[1] , **M. Morlighem**[1] , **J. Mouginot**[1,3] , and **H. Seroussi**[2]

[1]Department of Earth System Science, University of California, CA, Irvine, USA, [2]Jet Propulsion Laboratory, California Institute of Technology, CA, Pasadena, USA, [3]University of Grenoble Alpes, CNRS, IRD, Grenoble INP, IGE, Grenoble, France

Abstract In recent decades, tidewater glaciers in Northwest Greenland contributed significantly to sea level rise but exhibited a complex spatial pattern of retreat. Here we use novel observations of bathymetry and water temperature from NASA's Ocean Melting Greenland mission to quantify the role of warm, salty Atlantic Water in controlling the evolution of 37 glaciers. Modeled ocean-induced undercutting of calving margins compared with ice advection and ice front retreat observed by satellites from 1985 to 2015 indicate that 35 glaciers retreated when cumulative anomalies in ocean-induced undercutting rose above the range of seasonal variability of calving-front positions, while two glaciers standing on shallow sills and colder water did not retreat. Deviations in the observed timing of retreat are explained by residual uncertainties in bathymetry, inefficient mixing of waters in shallow fjords, and the presence of small floating sections. Overall, warmer ocean temperature triggered the retreat, but calving processes dominate ablation (71%).

Plain Language Summary In recent decades, tidewater glaciers in Northwest Greenland have contributed significantly to sea level rise but also exhibited a complex spatial pattern of retreat that remained unexplained. Here we use NASA's Oceans Melting Greenland (OMG) data in combination with the Estimating the Circulation and Climate of the Ocean (ECCO) ocean model outputs to assess the role of the ocean in triggering the retreat of these glaciers. We find that the timing of glacier retreat coincides with the timing of increased ocean-induced melting of the ice faces above average, which is driven by increases in ocean temperature and surface melt. While glacier retreat is initiated by the ocean, the calving of icebergs remains the dominant process of mass loss at the ice fronts (71%). The speed of retreat varies strongly with the slope of the glacier bed: fast retreats occur in deep fjords exposed to warm water and slow retreats in shallow fjords with cold water. These results vastly improve our understanding of the dominant role of ice-ocean interactions on the mass balance of the Greenland ice sheet.

1. Introduction

From 1991 to 2015, the mass loss from the Greenland Ice Sheet averaged 171 Gt/year or 0.47 mm/year sea level rise equivalent (Van den Broeke et al., 2016). Estimates from the Gravity Recovery and Climate Experiment reveal that nearly one third of the mass loss from 2003 to 2013 is from the northwest, principally from dynamic changes in marine-terminating glaciers (Velicogna et al., 2014). Coincident with this mass loss, oceanic (Rignot et al., 2012) and atmospheric (Hanna et al., 2012) temperatures have increased markedly in the northwest and many glacier fronts have retreated, some abruptly (Carr et al., 2013; Moon & Joughin, 2008; Moon et al., 2015; Murray et al., 2015). While oceanic and atmospheric forcings vary slowly with latitude along the coast (Figure 1), the pattern of retreat varied dramatically from one glacier to the next (Murray, Scharrer, et al., 2015).

Several hypotheses have been proposed to explain the variability in glacier response to climate warming, including differences in glacier/fjord geometry (Felikson et al., 2017; Kehrl et al., 2017; Meier & Post, 1987; Porter et al., 2014), atmospheric warming (Moon & Joughin, 2008), subglacial discharge (Bartholomaus et al., 2016; Motyka et al., 2013; Xu et al., 2013), and ocean-induced melting (Larsen et al., 2016; Rignot et al., 2010, 2016). These analyses suggest a complex interplay between bed topography, enhanced runoff due to atmospheric warming, enhanced ocean-induced ice melt due to ocean warming, and the supply of ice from upstream. Until recently, however, the glaciers in northwest Greenland had only been sparsely surveyed, little was known about the depth of the ice margin and glacial fjords, and ocean temperature in and out of the fjords.
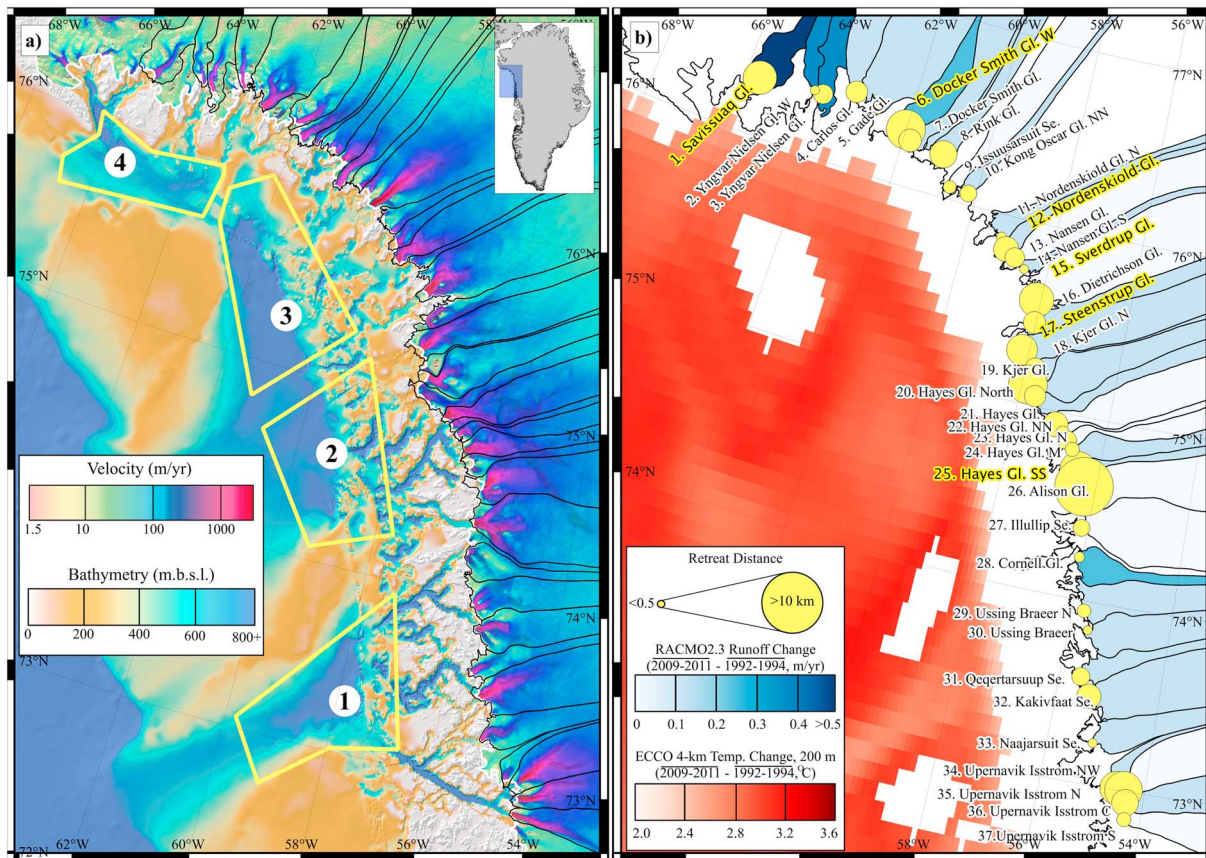
Figure 1. (a) Surface speed on grounded ice and bathymetry off shore, Northwest Greenland. Areas 1–4 indicate sample boxes used to extract ocean thermal forcing from the ECCO models. Glacier drainage basins are black lines. (b) Retreat distance (circle area) of 37 glaciers. Yellow names indicate glaciers discussed in Figure 2. Increase in annual runoff from the 1992–1994 mean to the 2009–2011 mean is color coded on grounded ice for each basin. Increase in ocean temperature below 200-m depth from the 1992–1994 mean to the 2009–2011 mean derived from ECCO models is color coded in red off shore; white areas have water depths less than 200 m. ECCO = Estimating the Circulation and Climate of the Ocean.

In the summer of 2015, NASA launched the Earth Suborbital Venture 2 (EVS-2) mission 'Oceans Melting Greenland (OMG) to measure bathymetry, surface topography, and ocean physical properties (temperature, salinity) along the ice sheet periphery (Fenty et al., 2016). OMG collected bathymetry data in many fjords that had never been surveyed before. The OMG bathymetric data have been combined with other data into BedMachine Version 3 (BM3), which is a comprehensive bed elevation map of the ice sheet and surrounding ocean (Morlighem et al., 2017).

Here we use OMG data, in combination with reconstructions of ice sheet runoff from the regional atmospheric climate model (RACMO2.3; Noël et al., 2016), ocean temperature and salinity from two Estimating the Circulation and Climate of the Ocean (ECCO) models (Forget et al., 2015; Menemenlis et al., 2008), ocean temperature from OMG in year 2015 (Fenty et al., 2016), and a parameterization of the rate of ice front undercutting by ocean waters based on high-resolution, MITgcm ocean model simulations (Rignot et al., 2016). We extend this approach evaluated for five glaciers in central West Greenland (Rignot et al., 2016) to 37 glaciers controlling the majority of the ice discharge in Northwest Greenland. We compare the results with the history of glacier fronts and ice front velocity from the mid-1980s to draw conclusions regarding the influence of ice-ocean interactions on the evolution of marine-terminating glaciers.

2. Methods and Data

In this study, we apply mass conservation across entire glacier fronts, that is, we consider mass fluxes per unit area, expressed in meters per day, which represent values averaged over the glacier width. The retreat rate, $\dot{q}_r$, of a glacier front averaged over its width is the result of three competing processes: (1) the advection of ice from upstream, $\dot{q}_f$, (2) ice front ocean-induced undercutting, $\dot{q}_m$, and (3) *dry* calving, $\dot{q}_c$, that is, $\dot{q}_r = \dot{q}_m + \dot{q}_c - \dot{q}_f$

(Rignot et al., 2016). We neglect the influence of surface melt. Surface melt does not impact ice front retreat when the glaciers are grounded, which is the case here for the vast majority of the glaciers (Table S1 in the supporting information). For glaciers developing a small floating section, the impact of surface thinning is discussed later on.

We denote by q_r the cumulative retreat of the glacier front, that is, the integration of $\dot{q}_r$ over time, and q_m^{anom} the cumulative anomaly in ocean-induced undercutting above a reference state. If $\dot{q}_f$ is greater (less) than the sum of $\dot{q}_m$ and $\dot{q}_c$, the glacier will advance (retreat). The $\dot{q}_r$ values are positive in the upstream direction, that is, $\dot{q}_r$ is negative when the glacier advances. We calculate $\dot{q}_r$ by digitizing ice front positions over time and $\dot{q}_m$ using a parameterized model of ice-ocean undercutting based on simulations by the MITgcm ocean model (Rignot et al., 2016; Xu et al., 2013). The parameterized model is constrained by reconstructions of ocean temperature from the ECCO2 (Menemenlis et al., 2008) and LLC270 (Forget et al., 2015) simulations, water depth from OMG bathymetry data, and subglacial discharge from RACMO2.3 and ISSM. We measure $\dot{q}_f$ annually from satellite data. The $\dot{q}_c$ is calculated as a residual from the mass conservation equation.

Ice front position, q_r, is digitized from Level 1 Landsat products spanning from the mid-1980s to 2016, in addition to those from Murray, Scharrer, et al. (2015) for 2000–2010 and Moon and Joughin (2008) for 2000, 2005–2017. To calculate glacier retreat, we employ the *box method* (Moon & Joughin, 2008); that is, we calculate the total change in glacier surface area, divide it by the average fjord width, and deduce a retreat distance, similar to Moon and Joughin (2008) and Howat and Eddy (2011), to obtain a time series of q_r. Uncertainty in ice front position varies from 30 m for Landsat 5/7 to 15 m for Landsat 8.

Ice front positions vary seasonally, generally advancing in winter and retreating in summer. To quantify this variability, we measure the standard deviation of the seasonal migration of each ice front, q_r^{ref}, for the years 1992 to 1997 when most glaciers were relatively stable. In the northern part of Melville Bay, where we do not have sufficient data, we use values for other glaciers similar in speed and fjord geometry (Table S1). We find a mean seasonal fluctuation of ±195 m, which compares well with ±220 m from Moon and Joughin (2008) and ±200 m by (Carr et al., 2013). We assume that any perturbation to the glacier front that keeps it within this range of variability will not affect the glacier stability. Conversely, a perturbation that migrates the ice front beyond that range of variability will trigger a glacier adjustment; that is, the glacier will dislodge from a stabilizing sill or retreat. The goal is to investigate whether an increase in q_m^{anom} above q_r^{ref} triggers a glacier retreat.

Ice velocity, $\dot{q}_f$, is estimated using feature-tracking, speckle-tracking, and radar interferometry on Landsat and radar observations (Howat, 2016; Joughin et al., 2010; Mouginot et al., 2017; Rignot & Kanagaratnam, 2006; Rignot & Mouginot, 2012; Rignot et al., 2016) by averaging observations within 1 year weighted by their uncertainty. One year spans from July 1 to June 30 since most radar-derived velocity data are acquired in winter. Seasonal fluctuations in ice velocity are at the 10% level (Moon et al., 2015), which introduces a bias of less than 2% on the annual average. Annual speed is extracted over the entire glacier width along a line parallel to the terminus position and 1 km upstream.

Ocean-induced undercutting, $\dot{q}_m$, is calculated using a parametric model as $(Ah\dot{q}_{sg}^{\alpha} + B)TF^{\beta}$, where h is water depth, $\dot{q}_{sg}$ subglacial discharge, TF thermal forcing from the ocean, and A, B, α, and β are constants (Rignot et al., 2016). The upper part (∼20% of the water column) of the glacier below the water line is not affected by the ocean (Fried et al., 2015; Rignot et al., 2015), does not buttress ice upstream, and typically sheds off the ice face. In effect, this parameterization also encapsulates ice loss which occurs above the undercut region of the ice face. What is not calved off from undercutting is removed by *dry calving*, that is, processes including the propagation of surface (Nick et al., 2010) or bottom cracks (Murray, Selmes, et al., 2015) to sea level, ice face shedding, and the rotation of ice blocks that detach from the front and produce icebergs. Here $\dot{q}_c$ is not modeled but deduced from the mass balance equation. We calculate the cumulative anomaly in ocean-induced melt, q_m^{anom}, from a reference state taken as the mean value of $\dot{q}_m$ for 1992–1997 when most glaciers were stable.

Water depth, h, is from OMG bathymetry (Oceans Melting Greenland, OMG, 2016a) using multibeam echo sounding. In Upernavik Isfjord and Alison Gl. fjord, brash ice conditions prevented complete boat surveys, so we use airborne gravity instead (OMG, 2016b) to yield bathymetry with a precision of 60 m (Millan et al., 2018).

Subglacial discharge, $\dot{q}_{sg}$, combines ice sheet surface runoff in the summer months from RACMO2.3 (Noël et al., 2016) with basal melting inland year round (Seroussi et al., 2013; Xu et al., 2012). Runoff production

is calculated over entire drainage basins and assumed to emerge at the ice front base instantaneously (Xu et al., 2012).

Ocean thermal forcing, *TF*, is the depth-integrated difference between the potential temperature of seawater and its salinity- and pressure-dependent freezing point (Xu et al., 2012). For ocean temperature and salinity, we combine the model output from the ECCO 4-km simulation of the Arctic Ocean for 1992 to 2011 (Rignot et al., 2012) with the output from ECCO LLC270 for 2000 to 2015. The ECCO 4-km solution captures the off-the-shelf/on-the-shelf heat transfer but does not employ off-the-shelf data assimilation. This solution has a −1°C bias (i.e., too cold) at the start of the simulation but agrees with observations in northeast Baffin Bay at the end in 2011; hence, we remove a bias which decreases linearly from −1°C in 1992 to 0°C in 2011. The ECCO LLC270 solution does not have enough resolution to resolve off-the-shelf/on-the-shelf heat transfer but is constrained by off-the-shelf observations. We adjust the LLC270 solution to match the 2015 conductivity-temperature-depth (CTD) data with a bias of −1.68 ± 0.32°C, that is, the LLC270 solution is too cold. As the ECCO models did not use correct bathymetry in the fjords (Jakobsson et al., 2012), we extract temperature at the fjord entrance and on the continental shelf in four areas (Figure 1). We include samples at least as deep as the fjords to encapsulate deep troughs not known prior to OMG (OMG, 2016a). We average vertical profiles horizontally within each domain to define an average vertical profile of waters capable of entering the fjords. We assume no heat loss between the sample domain and the fjord entrance. We merge the ECCO 4-km and LLC270 solutions over the 2009–2011 common period using a linear combination to transition smoothly between solutions.

We compare CTDs within the sample domains with CTDs near the glacier fronts to characterize the transfer function of *TF* due to sills, fjord constrictions, vertical/horizontal heat transfer, and other impedances that modify the water properties between the shelf and the fjord. We recognize that these shelf-fjord differences may vary seasonally and interannually, but we lack time series of CTDs to characterize such changes. We apply the CTD-derived, glacier-specific, and depth-dependent transfer functions to the model-derived *TF* on the shelf to obtain *TF* at the glacier termini for the time period 1992–2015. The transfer function is depth dependent and varies between fjords, with an average value of −0.41 ± 0.23°C for all fjords averaged over depth; that is, *TF* is lower in the fjords than on the continental shelf. Finally, we integrate *TF* across the glacier width.

Uncertainty in $\dot{q}_m$ arises from (1) a 7% error in model parameterization fit (Rignot et al., 2016), (2) a 5% uncertainty in submerged area of the glacier termini (Rignot et al., 2016), (3) a 15% uncertainty in size and location of subglacial discharge channels (Xu et al., 2013), and (4) uncertainties in h, q_{sg}, and *TF*. The uncertainty in h varies from fjord to fjord (Morlighem et al., 2017) but averages 35% because some fjords are not completely mapped. The uncertainty in q_{sg} is 20% (Noël et al., 2016). The uncertainty in *TF* is deduced from the error in the ECCO 4-km and LLC270 solutions and the transfer functions. We estimate it at 0.32°C based on the standard deviation between 2015 CTDs and the ECCO solutions. We propagate the uncertainty in h, q_{sg}, and *TF* quadratically with the other errors to obtain a total error in glacier undercutting, $\dot{q}_m$, of 26%, which is then used to estimate the cumulative error (Figures 2 and S1.X in the supporting information).

3. Results

Ice front migration from the 1992–1997 mean to 2016 ranges from a 110-m advance (Naajarsuit Se.) to a 21.2-km retreat (Alison Gl., which lost its ice shelf). The timing, rate, and magnitude of retreat vary significantly along the coastline, with no trend with latitude. Most glaciers, except Kjer Gl., maintained a constant ice front position from 1992 until about year 2000, with small seasonal and interannual variability. 35 glaciers underwent a retreat, that is, $q_r > q_r^{ref}$, during that period, while two glaciers remained stable.

The mean summertime (July to August) subglacial discharge varied from 7 (Carlos Gl.) to 96 m³/s (Kakiffaat Se.) for the 37 glaciers. The annual average subglacial discharge increased by 85% on average from 1992 to 2015. Similarly, *TF* increased by 2.18 ± 0.44°C on average from 1992 to 2011 (Figure 1). CTDs taken during the OMG campaign in 2015 indicate waters 1°C cooler than in 2011. The increases in $\dot{q}_{sg}$ and *TF* increase the modeled $\dot{q}_m$, with peak values for peak *TF* in 2010. The modeled $\dot{q}_m$ and observed ablation ($\dot{q}_f + \dot{q}_r$) indicate that ice font undercutting accounted for 29% of the total ablation of the 37 glaciers from 1992 to 2015 (Table S2) vs 71% for $\dot{q}_c$, which therefore accounts for the majority of the retreat. Comparing *TF* and $\dot{q}_{sg}$, we find that the change in *TF* accounts for 98% of q_m^{anom} on average versus 2% for $\dot{q}_{sg}$, i.e., *TF* dominates the long-term increase in $\dot{q}_m$. We now discuss 6 representative glaciers, with numbers shown in Figure 2 and Table S2.
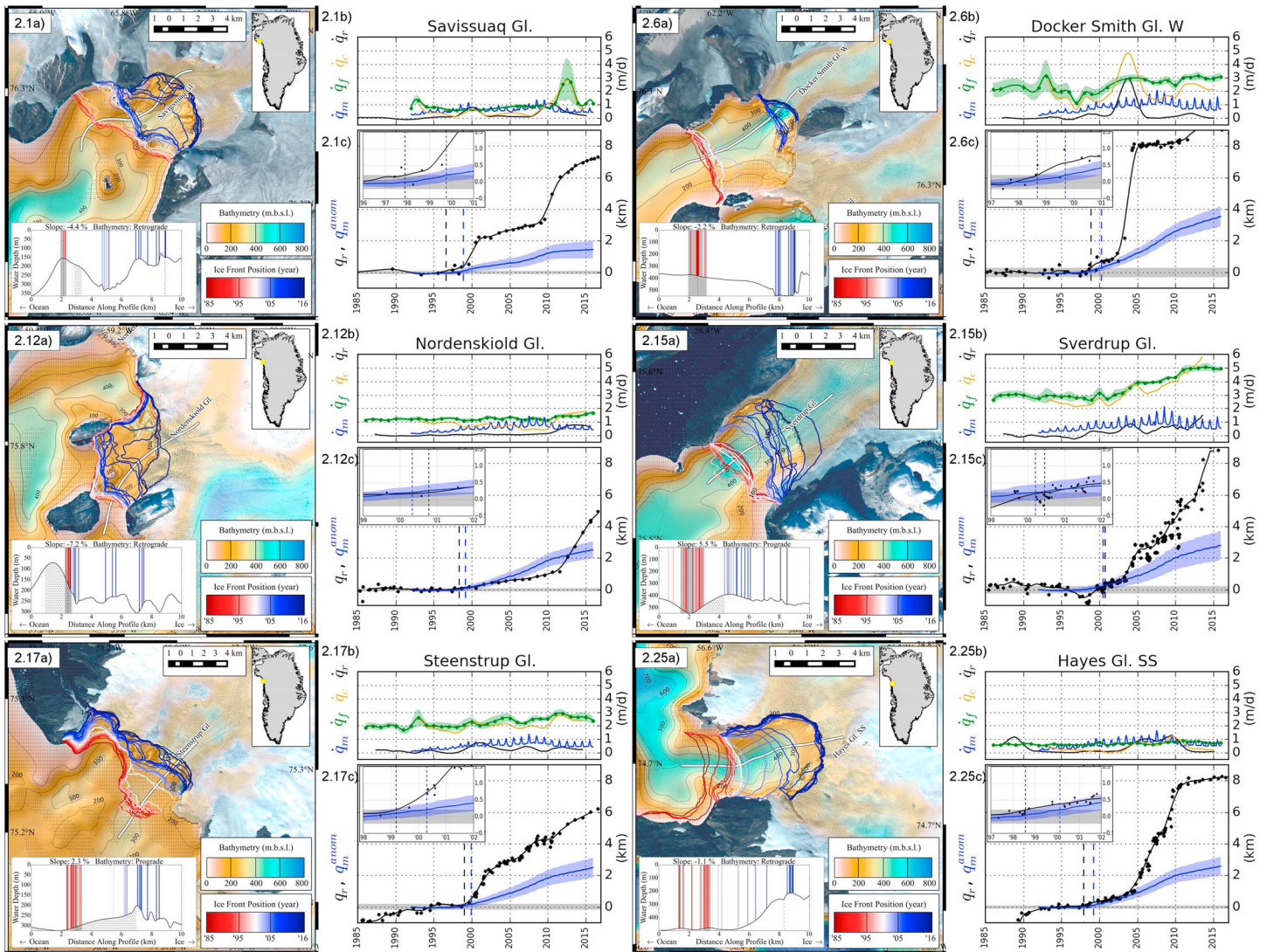
Figure 2. Western branch of Savissuaq Gl., Døcker Smith Gl. W, Nordenskiöld Gl., Sverdrup Gl., Steenstrup Gl., and southern branch of Hayes Gl. (a) Bathymetry from BM3 and historical ice front positions. Stipples indicate interpolated bathymetry. Inset shows the glacier profile along the 10-km white line, with calving-front positions and the value of q_r^{ref}. (b) Rates of undercutting (blue), ice front speed (green), calving rate (brown), and retreat rate (black). (c) Cumulative anomaly in undercutting (blue) and ice front retreat (black). The envelope of natural variability is grey. The black dotted line indicates $q_r > q_r^{ref}$. The blue dotted line indicates $q_m^{anom} > q_r^{ref}$. Insets on (c) are expanded views of the timing of retreat.

Savissuaq Gl. (#1), at the western end of Melville Bay (76.3°N, 65.7°W), terminates in a fjord 200–300-m deep. Until 1999, Savissuaq Gl. was pinned on a sharp and shallow protrusion. From 1999 to 2010, $\dot{q}_f$ and $\dot{q}_m$ increased by 0.5 m/day to 1 m/day and 1.2 m/day, respectively, and the glacier retreated off the pinning point by 4 km along a retrograde slope before stabilizing on a shallower, prograde slope. As the front stabilized, the $\dot{q}_m$ value dropped to 0.5 m/day, respectively. For 1992–2015, q_m accounts for 46% ± 8% of the total ablation.

Døcker Smith Gl., east of Savissuaq Gl., splits into two branches around a nunatak. The western branch, Døcker Smith Gl. W, (#6; 76.3°N, 62.0°W) is 300–400-m deep, with a 500-m-deep fjord at the center. From 1985 to 2002, the terminus underwent small seasonal fluctuations on a shallow (200–300 m) section of the fjord. In 2003–2004, the terminus retreated by 5 km along a retrograde slope, deepening by 100 m. During the retreat, $\dot{q}_m$ increased by 0.5 m/day, $\dot{q}_c$ tripled, $\dot{q}_f$ accelerated from 2 to 3 m/day, and Døcker Smith Gl. W detached from the main branch. After the retreat, the glacier front restabilized in a fjord constriction, $\dot{q}_c$ decreased, and the ice velocity remained constant. For 1992–2015, q_m accounts for 27 ± 4% of the total ablation.

Nordenskiöld Gl (#12; 75.8°N, 59.1°W) in southern Melville Bay terminates in a 200- to 300-m-deep fjord. From 1985 to 1999, the ice front was pinned between two islands. In 2000, $\dot{q}_m$ increased from 0.5 to 1 m/day,
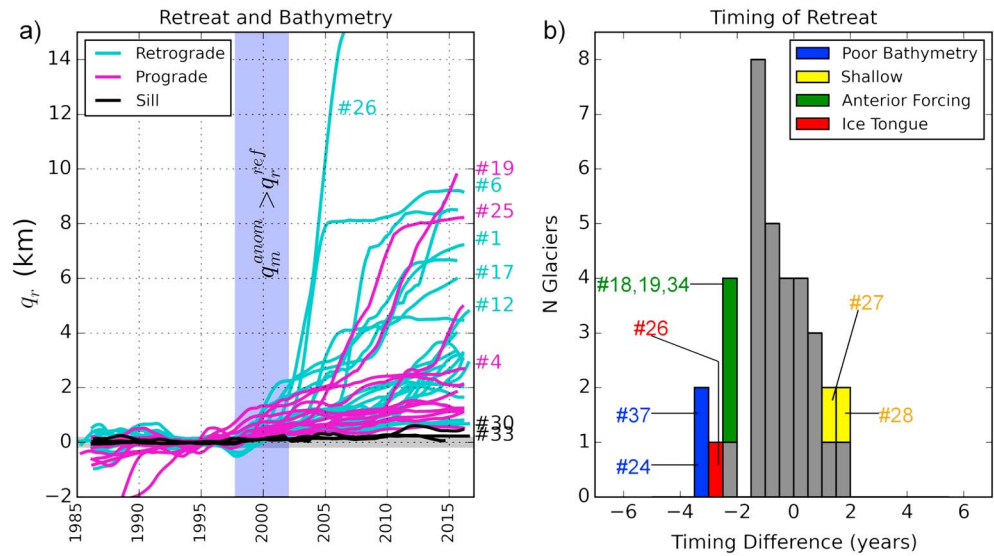
Figure 3. (a) History of ice front positions for 37 glaciers. The blue band denotes $q_m^{anom} > q_r^{ref}$. Bed slope is magenta for prograde and teal for retrograde, measured for the mean front position 1992–1997. Glacier numbers from Figure 1: (1) Savissuaq, (4) Carlos, (6) Døcker Smith W, (12) Nordenskiöld, (17) Steenstrup, (19) Kjer, (25) Hayes SS, (26) Alison, (30) Ussing Bræer, and (33) Naajarsuit glaciers. (b) Histogram of the difference in timing between q_m^{anom} and q_r. Colors indicate cases identified in the text. Anterior forcing refers to cases where the ice front retreat is influenced by an adjacent glacier or the glacier was already retreating prior to our time span of investigation.

the ice front detached from one island and retreated. As $\dot{q}_m$ increased between 2000 and 2010 to 1.3 m/day, $\dot{q}_f$ remained constant at 1.5 m/day, while $\dot{q}_c$ decreased from 1 to 0.8 m/day. In 2010, the ice front separated from the second island and $\dot{q}_f$ increased to 2 m/day. For 1992 to 2015, q_m accounts for 37% $\pm$ 5% of the total ablation.

Sverdrup Gl. (#15; 75.6°N, 58.2°W), south of Nordenskiöld Gl., terminates in a narrow fjord 400- to 500-m deep. From the mid-1980s until the early 2000s, the ice front position fluctuated by $\pm$220 m. Since 1991, the velocity remained constant at 3 m/day until 2002 when the ice front retreated slowly and $\dot{q}_m$, $\dot{q}_c$, and $\dot{q}_f$ increased. At the end of 2015, ice velocity was 5 m/day, with ongoing retreat. During 1992–2015, q_m accounts for 18% $\pm$ 3% of the total ablation.

Steenstrup Gl. (#17; 75.3°N, 58.0°W), south of Sverdrup Gl., is a 12-km-wide glacier terminating in a broad fjord between a rocky outcrop and a small island. After a 1-km retreat between 1985 and 1990, Steenstrup remained stable on a shallow (200–300 m) bed. From 1992 to 1999, $\dot{q}_m$ increased fourfold from 0.2 to 0.8 m/day and the glacier retreated 6 km from 1999 to 2015 across a relatively flat bed. q_m accounts for 23% $\pm$ 4% of the ice front loss.

The Hayes Region, 100 km south of Steenstrup Gl., is a large system which splinters into six outlets around protruding rocks and islands. The southernmost branch, Hayes Gl. SS, (#25; 74.7°N, 56.5°W) flows into a 5-km-wide fjord behind large islands. The ice front retreated 4 km from 1985 to 1991 and stabilized in a fjord constriction. After that, $\dot{q}_f$ remained constant, and q_r varied within 650 m. Following a few years of enhanced melt in 1997–2000, the ice front retreated until the bed shoaled from 500 to 200 m. $\dot{q}_m$ dropped significantly, the ice velocity decreased, and the ice front stabilized. q_m accounts for 65% $\pm$ 8% of the mass ablation (Table S1 and Figure S2).

4. Discussion

Ocean-triggered retreats, that is, when $q_m^{anom} > q_r^{ref}$, is detected for 33 glaciers. At that time, q_m^{anom} is large enough to push the glacier front beyond the natural range of variability and force it to a new state. The rate of glacier retreat varies with the slope of the bed (Figure 3), which we measure along the center line (Figure 2 and S2). Larger retreat is associated with retrograde slopes (67% of 33 glaciers) and smaller retreat with prograde slopes (33% of 33 glaciers). The mean retreat distance relative to the 1992–1997 position is 5.0 km for retrograde slopes versus 3.1 km for prograde slopes.

While our results suggest that ocean undercutting triggers the retreat, we note that the dominant ablation process is $\dot{q}_c$, which accounts for 71% $\pm$ 9% of the total ablation on average versus 29% $\pm$ 4% for $\dot{q}_m$ (Table S2). The $\dot{q}_c$ responds to changes in the stress field caused by the increase in glacier speed, $\dot{q}_f$. Conversely, if $\dot{q}_c$ did not change, the impact of the ocean on the glacial retreat would have been much less.

The timing of retreat is not detected better than within 1 year because the process is slow, affected by natural variability, and dependent on q_r^{ref}. For Savissuaq and Steenstrup, the retreat ensued abruptly, while for Døcker Smith W the retreat started slowly when $q_m^{\text{anom}} > q_r^{\text{ref}}$ by a few 100 m, and then abruptly increased. For Nordenskiöld, Sverdrup, and Hayes SS, q_m^{anom} exceeded q_r^{ref} after 2000 but the ice front retreated later, because q_r^{ref} is underestimated or q_m^{anom} is overestimated. For Savissuaq, Døcker Smith W and Hayes SS, the retreat slowed as the ice front reached fjord constrictions and shallower bathymetry. For Nordenskiöld, Sverdrup, and Steenstrup, the retreat was more steady because of a relatively uniform bathymetry.

The mismatch between the timing of retreat and the increase in q_m^{anom} is within uncertainty bounds for all but six glaciers, which changed sooner: Kjer Gl. N (#18), Kjer Gl (#19), Hayes M (#24), Alison Gl. (#26), Upernavik Isstrøm NW (#34), and Upernavik Isstrøm S (#37)) (Figure 3). Several factors contribute to the apparent inconsistency. For Upernavik Isstrøm NW (#34), the glacier merged with Upernavik Isstrøm N (#35) prior to 2007. As Upernavik Isstrøm N retreated, Upernavik Isstrøm NW lost contact along one side margin, retreated, and sped up, not due to a change in ocean conditions, but due to changes along one shear margin. For Kjer Gl., the retreat started prior to 1992, so the reference level q_r^{ref} is likely overestimated. The glacier was also affected by the retreat of the adjacent Kjer Gl. N, similar to Upernavik Isstrøm NW. For Alison Gl. (#26), the retreat is associated with the collapse of its ice tongue in 2004, similar to Jakobshavn Isbræ (Podlech & Weidick, 2004). Our parametrization of $\dot{q}_m$ for vertical calving walls may not apply to that geometry, hindering our assessment. For Upernavik Isstrøm S (#37) and Hayes M. (#24), the bathymetry is incomplete, the transport of ocean heat appears to be overestimated from our interpolated bathymetry (Figure 3).

Two glaciers experienced a delayed response. Illullip Se. (#27) has maintained a stable ice front in cold waters less than 300-m deep, with $\dot{q}_f$ much larger than $\dot{q}_m$. CTDs from OMG indicate that the waters in Ryders Fjord near Cornell Gl. (#28) do not experience vigorous vertical mixing with Atlantic Waters and remain cold (Fenty et al., 2016), which implies that our modeled $\dot{q}_m$ overestimates undercutting. In these fjords, the Atlantic Water layer is thinner than in other fjords and our parameterization overestimates the amount of ocean heat available to undercut the glacier.

Three glaciers — Nansen Gl. S (#14), Naajarsuit Se. (#33), and Ussing Bræer (#30) — displayed minor ice front perturbations in the last 30 years. Naajarsuit Se. terminates in a fjord constriction, with a bed less than 200-m deep. We calculate that q_m^{anom} exceeded q_r^{ref} in the late 1990s, $\dot{q}_f$ declined, yet the glacier remained stable. A similar behavior is observed for Nansen Gl. S and Ussing Bræer. In these fjords, the ice fronts are grounded on shallow, narrow sills. They develop small floating sections that break up and rotate off the ice face. This form of calving is not affected by undercutting since the ice blocks detach upstream of the line of undercutting (Murray, Selmes, et al., 2015).

Except for glaciers standing in shallow waters, already in a state of retreat, calving on a narrow sills, or with residual uncertainties in bathymetry, we find a remarkable agreement between the timing of retreat and the timing of enhanced $\dot{q}_m$. Once the retreat is initiated, the magnitude of the retreat depends on bed slope, consistent with the tidewater glacier cycle (Meier & Post, 1987). Among the glaciers experiencing rapid retreat, only three did not initiate retreat along a retrograde bed: Sverdrup Gl., Steenstrup Gl., and Upernavik Isstrøm NW. BM3 indicates a shoaling of more than 20% for Sverdrup and Steenstrup, but the bathymetry in that region is interpolated. The two branches of Upernavik Isstrøm discussed previously have wide overdeepenings upstream. Illullip Se. and Ussing Bræer N experienced small abrupt retreats because of the presence of small, deep sections near the ice front.

While our results demonstrate a strong relationship between increased ocean-induced undercutting and glacier retreat, other factors may be important, including calving enhancement from weaker ice mélange (Moon et al., 2015) and surface thinning (Csatho et al., 2014). Moon et al. (2015) find that seasonal retreat is greater during periods of weak mélange or open water fjords, and persistence of such conditions may contribute to ice front retreat due to enhanced calving activity. This process would translate into an increase in $\dot{q}_c$. The stability of the glaciers may also be affected by surface thinning, which brings ice fronts closer to floatation. We analyzed the elevation above floatation of all glacier fronts in 1985 (Korsgaard et al., 2016)

and 2002 (Howat et al., 2014). Nearly all glaciers have small or negligible floating sections in Northwest Greenland, except six: Docker Smith Gl. W, Rink Gl., Hayes Gl., Hayes Gl. SS, Alison Gl., and Upernavik Isstrøm N. For these glaciers, the rate of retreat associated with a 1-m/year thinning using the relationship between thinning and grounding line retreat in Thomas and Bentley (1978) is several times smaller than that calculated for ocean-induced undercutting. One exception is Rink if the glacier would thin by 1 m/year or more, but Rink has insofar remained stable.

This interpretation of glacier evolution was made possible from new bathymetry and ocean temperature data. A few fjords remain incompletely mapped: Kong Oscar, Steenstrup, Hayes, and Kakiffaat. We omit Kong Oscar from our analysis due to large uncertainties in bathymetry. We recommend that bathymetry mapping be completed around the entire periphery of Greenland. The results will be critical to improve projections of sea level change from Greenland glaciers.

5. Conclusions

We assess the evolution of the ice fronts of northwest tidewater glaciers versus the rates of ice advection, ocean-induced melt, and dry calving processes. We calculate the rates of subaqueous undercutting using model-derived ocean thermal forcing, subglacial discharge, bed geometry, and a parameterized model of glacier undercutting. The results indicate that ocean warming below 200-m depth has very likely triggered the vast majority of the glacier retreat. Glaciers that did not retreat stand on shallow sills in cold water. Other exceptions are associated with uncertainties in bathymetry and the presence of small floating sections. This study therefore establishes a strong quantitative link between ocean thermal forcing and tidewater glacier evolution. Another conclusion is that *dry calving* remains a dominant process of mass ablation at calving margins, so that it remains critical to improve our understanding of the calving mechanics of Greenland glaciers.

Notation

The following list of terms, in order of appearance, is provided for clarity.

1. $\dot{q}_r$, linear rate of ice front retreat (m/day).
2. q_r, linear ice front retreat distance (m).
3. q_r^{ref}, mean seasonal fluctuations of the ice front 1992–1997 (m).
4. $\dot{q}_f$, ice front velocity (m/day).
5. $\dot{q}_m$, ocean-induced undercutting (m/day).
6. q_m^{anom}, cumulative anomalous melt, that is, the integration of $\dot{q}_m$, relative to the 1992–1997 mean.
7. $\dot{q}_{sg}$, subglacial discharge at the glacier terminus.

References

Bartholomaus, T. C., Stearns, L. A., Sutherland, D. A., Shroyer, E. L., Nash, J. D., Walker, R. T., et al. (2016). Contrasts in the response of adjacent fjords and glaciers to ice-sheet surface melt in west greenland. *Annals of Glaciology*, 57(73), 25–38.

Carr, J. R., Vieli, A., & Stokes, C. (2013). Influence of sea ice decline, atmospheric warming, and glacier width on marine-terminating outlet glacier behavior in Northwest Greenland at seasonal to interannual timescales. *Journal of Geophysical Research: Earth Surface*, 118, 1210–1226. https://doi.org/10.1002/jgrf.20088

Csatho, B. M., Schenk, A. F., van der Veen, C. J., Babonis, G., Duncan, K., Rezvanbehbahani, S., et al. (2014). Laser altimetry reveals complex pattern of Greenland ice sheet dynamics. *Proceedings of the National Academy of Sciences*, 111(52), 18,478–18,483.

Felikson, D., Bartholomaus, T. C., Catania, G. A., Korsgaard, N. J., Kjær, K. H., Morlighem, M., et al. (2017). Inland thinning on the Greenland ice sheet controlled by outlet glacier geometry. *Nature Geoscience*, 10(5), 366–369.

Fenty, I., Willis, J. K., Khazendar, A., Dinardo, S., Forsberg, R., Fukumori, I., et al. (2016). Oceans melting greenland: Early results from NASA's ocean-ice mission in Greenland. *Oceanography*, 29(4), 72–83.

Forget, G., Campin, J., Heimbach, P., Hill, C., Ponte, R., & Wunsch, C. (2015). ECCO version 4: An integrated framework for non-linear inverse modeling and global ocean state estimation. *Geoscientific Model Development*, 8(10), 3071.

Fried, M., Catania, G., Bartholomaus, T., Duncan, D., Davis, M., Stearns, L., et al. (2015). Distributed subglacial discharge drives significant submarine melt at a Greenland tidewater glacier. *Geophysical Research Letters*, 42, 9328–9336. https://doi.org/10.1002/2015GL065806

Hanna, E., Mernild, S. H., Cappelen, J., & Steffen, K. (2012). Recent warming in Greenland in a long-term instrumental (1881–2012) climatic context: I. Evaluation of surface air temperature records. *Environmental Research Letters*, 7(4), 045404.

Howat, I. (2016). Measures Greenland ice velocity: Selected glacier site velocity maps from optical images, version 1 (Tech. Rep.). NASA National Snow and Ice Data Center Distributed Active Archive Center.

Howat, I. M., & Eddy, A. (2011). Multi-decadal retreat of Greenland's marine-terminating glaciers. *Journal of Glaciology*, 57(203), 389–396.

Howat, I., Negrete, A., & Smith, B. (2014). The Greenland ice mapping project (GIMP) land classification and surface elevation data sets. *The Cryosphere*, 8(4), 1509–1518.

Jakobsson, M., Mayer, L., Coakley, B., Dowdeswell, J. A., Forbes, S., Fridman, B., et al. (2012). The International Bathymetric Chart of the Arctic Ocean (IBCAO) version 3.0. *Geophysical Research Letters*, *39*, L12609. https://doi.org/10.1029/2012GL052219

Joughin, I., Smith, B. E., Howat, I. M., Scambos, T., & Moon, T. (2010). Greenland flow variability from ice-sheet-wide velocity mapping. *Journal of Glaciology*, *56*(197), 415–430.

Kehrl, L., Joughin, I., Shean, D., Floricioiu, D., & Krieger, L. (2017). Seasonal and interannual variabilities in terminus position, glacier velocity, and surface elevation at Helheim and Kangerlussuaq Glaciers from 2008 to 2016. *Journal of Geophysical Research: Earth Surface*, *122*, 1635–1652. https://doi.org/10.1002/2016JF004133

Korsgaard, N. J., Nuth, C., Khan, S. A., Kjeldsen, K. K., Bjørk, A. A., Schomacker, A., & Kjær, K. H. (2016). Digital elevation model and orthophotographs of Greenland based on aerial photographs from 1978–1987. *Scientific Data*, *3*, 160032.

Larsen, S. H., Khan, S. A., Ahlstrøm, A. P., Hvidberg, C. S., Willis, M. J., & Andersen, S. B. (2016). Increased mass loss and asynchronous behavior of marine-terminating outlet glaciers at Upernavik IsstrØm, NW Greenland. *Journal of Geophysical Research: Earth Surface*, *121*, 241–256. https://doi.org/10.1002/2015JF003507

Meier, M., & Post, A. (1987). Fast tidewater glaciers. *Journal of Geophysical Research*, *92*(B9), 9051–9058. https://doi.org/10.1029/JB092iB09p09051

Menemenlis, D., Campin, J.-M., Heimbach, P., Hill, C., Lee, T., Nguyen, A., et al. (2008). ECCO2: High resolution global ocean and sea ice data synthesis. *Mercator Ocean Quarterly Newsletter*, *31*, 13–21.

Millan, R., Rignot, E., Mouginot, J., Wood, M., Bjørk, A. A., & Morlighem, M. (2018). Vulnerability of southeast Greenland glaciers to warm Atlantic water from operation icebridge and ocean melting Greenland data. *Geophysical Research Letters*, *45*, 2688–2696. https://doi.org/10.1002/2017GL076561

Moon, T., & Joughin, I. (2008). Changes in ice front position on Greenland's outlet glaciers from 1992 to 2007. *Journal of Geophysical Research*, *113*, F02022. https://doi.org/10.1029/2007JF000927

Moon, T., Joughin, I., & Smith, B. (2015). Seasonal to multiyear variability of glacier surface velocity, terminus position, and sea ice/ice mélange in Northwest Greenland. *Journal of Geophysical Research: Earth Surface*, *120*, 818–833. https://doi.org/10.1002/2015JF003494

Morlighem, M., Williams, C. N., Rignot, E., An, L., Arndt, J., & Bamber, J. (2017). BedMachine v3: Complete bed topography and ocean bathymetry mapping of Greenland from multibeam echo sounding combined with mass conservation. *Geophysical Research Letters*, *44*, 11,051–11,061. https://doi.org/10.1002/2017GL074954

Motyka, R. J., Dryer, W. P., Amundson, J., Truffer, M., & Fahnestock, M. (2013). Rapid submarine melting driven by subglacial discharge, Leconte Glacier, Alaska. *Geophysical Research Letters*, *40*, 5153–5158. https://doi.org/10.1002/grl.51011

Mouginot, J., Rignot, E., Scheuchl, B., & Millan, R. (2017). Comprehensive annual ice sheet velocity mapping using Landsat-8, Sentinel-1, and RADARSAT-2 data. *Remote Sensing*, *9*, 364.

Murray, T., Scharrer, K., Selmes, N., Booth, A., James, T., Bevan, S., et al. (2015). Extensive retreat of Greenland tidewater glaciers, 2000–2010. *Arctic, Antarctic, and Alpine Research*, *47*, 427–447.

Murray, T., Selmes, N., James, T. D., Edwards, S., Martin, I., O'Farrell, T., et al. (2015). Dynamics of glacier calving at the ungrounded margin of Helheim Glacier, Southeast Greenland. *Journal of Geophysical Research: Earth Surface*, *120*, 964–982. https://doi.org/10.1002/2015JF003531

Nick, F., Van der Veen, C. J., Vieli, A., & Benn, D. (2010). A physically based calving model applied to marine outlet glaciers and implications for the glacier dynamics. *Journal of Glaciology*, *56*, 781–794.

Noël, B., van de Berg, W. J., Machguth, H., Howat, I., Fettweis, X., & van den Broeke, M. R. (2016). A daily, 1-km resolution data set of downscaled Greenland ice sheet surface mass balance (1958–2015). *The Cryosphere*, *10*, 2361.

OMG (2016a). OMG mission: Bathymetry (sea floor depth) data from the ship-based bathymetry survey. ver. 0.1 (Tech. Rep.). CA, USA.

OMG (2016b). Airborne gravity data from the airborne bathymetry survey. ver. 0.1 (Tech. Rep.). CA, USA.

Podlech, S., & Weidick, A. (2004). Catastrophic break-up of the front of Jakobshavn Isbræ, West Greenland, 2002/03. *Journal of Glaciology*, *50*, 153–154. https://doi.org/10.3189/172756504781830231

Porter, D. F., Tinto, K. J., Boghosian, A., Cochran, J. R., Bell, R. E., Manizade, S. S., & Sonntag, J. G. (2014). Bathymetric control of tidewater glacier mass loss in Northwest Greenland. *Earth and Planetary Science Letters*, *401*, 40–46.

Rignot, E., Fenty, I., Menemenlis, D., & Xu, Y. (2012). Spreading of warm ocean waters around Greenland as a possible cause for glacier acceleration. *Annals of Glaciology*, *53*, 257–266.

Rignot, E., Fenty, I., Xu, Y., Cai, C., & Kemp, C. (2015). Undercutting of marine-terminating glaciers in West Greenland. *Geophysical Research Letters*, *42*, 5909–5917. https://doi.org/10.1002/2015GL064236

Rignot, E., & Kanagaratnam, P. (2006). Changes in the velocity structure of the Greenland ice sheet. *Science*, *311*, 986–990.

Rignot, E., Koppes, M., & Velicogna, I. (2010). Rapid submarine melting of the calving faces of West Greenland glaciers. *Nature Geoscience*, *3*, 187–191.

Rignot, E., & Mouginot, J. (2012). Ice flow in Greenland for the international polar year 2008–2009. *Geophysical Research Letters*, *39*, L11501. https://doi.org/10.1029/2012GL051634

Rignot, E., Xu, Y., Mouginot, J., Scheuchl, B., & Li, X. (2016). Modeling of ocean-induced ice melt rates of five west greenland glaciers over the past two decades. *Geophysical Research Letters*, *43*, 6374–6382. https://doi.org/10.1002/2016GL068784

Seroussi, H., Morlighem, M., Rignot, E., Khazendar, A., Larour, E., & Mouginot, J. (2013). Dependence of century-scale projections of the Greenland ice sheet on its thermal regime. *Journal of Glaciology*, *59*, 1024–1034.

Thomas, R. H., & Bentley, C. R. (1978). A model for holocene retreat of the West Antarctic ice sheet. *Quaternary Research*, *10*(2), 150–170.

Van den Broeke, M. R., Enderlin, E. M., Howat, I. M., Munneke, K., Noël, B. P., & Jan Van De Berg, W. (2016). On the AQPlease check if the reference author Broeke (2016) is captured correctly.recent contribution of the Greenland ice sheet to sea level change. *The Cryosphere*, *10*, 1933–1946.

Velicogna, I., Sutterley, T., & Van den Broeke, M. (2014). Regional acceleration in ice mass loss from Greenland and Antarctica using GRACE time-variable gravity data. *Geophysical Research Letters*, *41*(22), 8130–8137. https://doi.org/https://doi.org/10.1002/2014GL061052

Xu, Y., Rignot, E., Fenty, I., Menemenlis, D., & Flexas, M. (2013). Subaqueous melting of Store glacier, west Greenland from three-dimensional, high-resolution numerical modeling and ocean observations. *Geophysical Research Letters*, *40*, 4648–4653. https://doi.org/10.1002/grl.50825

Xu, Y., Rignot, E., Menemenlis, D., & Koppes, M. (2012). Numerical experiments on subaqueous melting of Greenland tidewater glaciers in response to ocean warming and enhanced subglacial discharge. *Annals of Glaciology*, *53*(60), 229–234.